Opto-Electronic Advances

Original Article

2021, Vol. 4, No. 7

DOI: 10.29026/oea.2021.200088

Ultra-high extinction-ratio light modulation by electrically tunable metasurface using dual epsilon-near-zero resonances

Arash Nemati[1,2], Qian Wang[1], Norman Soo Seng Ang[1], Weide Wang[1], Minghui Hong[2] and Jinghua Teng[1]*

The lossy nature of indium tin oxide (ITO) at epsilon-near-zero (ENZ) wavelength is used to design an electrically tunable metasurface absorber. The metasurface unit cell is constructed of a circular resonator comprising two ITO discs and a high dielectric constant perovskite barium strontium titanate (BST) film. The ENZ wavelength in the accumulation and depletion layers of ITO discs is controlled by applying a single bias voltage. The coupling of magnetic dipole resonance with the ENZ wavelength inside the accumulation layer of ITO film causes total absorption of reflected light. The reflection amplitude can achieve ~84 dB or ~99.99% modulation depth in the operation wavelength of 820 nm at a bias voltage of −2.5 V. Moreover, the metasurface is insensitive to the polarization of the incident light due to the circular design of resonators and the symmetrical design of bias connections.

Keywords: metasurface; electrically tunable; indium tin oxide (ITO); epsilon-near-zero (ENZ); barium strontium titanate (BST); polarization-insensitive

Nemati A, Wang Q, Ang NSS, Wang WD, Hong MH et al. Ultra-high extinction-ratio light modulation by electrically tunable metasurface using dual epsilon-near-zero resonances. *Opto-Electron Adv* **4**, 200088 (2021).

Introduction

Metasurfaces are the two-dimensional equivalent of metamaterials, composing discrete subwavelength structures, possessing the capability of full control of light properties, such as amplitude, phase, dispersion, momentum, and polarization[1–7]. Metasurfaces are used in various applications covering electromagnetic spectra ranging from microwave, terahertz (THz), infrared, visible, to ultra-violet (UV)[8]. Active control of light propagation in visible and near-infrared (near-IR) spectra has practical and fundamental significance in autonomous vehicles, robots, display, augmented and virtual reality, consumer electronics, telecommunications, and sensing devices[9–14]. To tune a metasurface, we can change either the property of the unit cells or its ambient. This could be done by employing active materials in the metasurface, which can have their properties changed by an external stimulus. Each type of these materials has different properties and tuning mechanisms.

Transparent conductive oxides are optically transparent and electrically conductive. They have been widely used in photovoltaics, organic light-emitting diodes,

[1]Institute of Materials Research and Engineering, Agency for Science, Technology and Research (A*STAR), 2 Fusionopolis Way, Singapore 138634, Singapore; [2]Department of Electrical and Computer Engineering, National University of Singapore, Engineering Drive 3, Singapore 117576, Singapore.

*Correspondence: JH Teng, Email: jh-teng@imre.a-star.edu.sg

Received: 5 December 2020; Accepted: 25 March 2021; Published: 25 July 2021

displays, and electro-optics devices[15,16]. Recently, the tunable property of transparent conductive oxides, such as indium tin oxide (ITO), has attracted great attention for its applications in metasurfaces and flat optics[17]. Moreover, the tunability in ITO is a field-effect modulation mechanism that is based on the formation of charge depletion or accumulation regions. This gives them advantages of low power and high speed compared to the other common tuning mechanisms, such as MEMS, mechanical strain, liquid crystals, and phase change materials[9,18–20].

So far most of the focus in using tunable ITO film has been on designing beamsteering metasurfaces[21–23]. To tune the electron density and optical constants in the ITO film, different structures have been proposed. A 300° phase change was shown in a reflective dual-gate metasurface structure using a single ITO film with the measured reflectance below 30%[22]. Recently, over 360° phase change and a scan angle of 8° with a deflection efficiency of 34% were achieved[24]. Although the strong resonance and electric and magnetic confinement in the ITO film has been very beneficial to achieving high phase change, it has limited the achievable efficiency.

Hence, ITO could be a better candidate for modulation of light intensity by playing with its plasmonic resonance. An electrically tunable metasurface working as a modulator could not only benefit from the fast tunability of ITO but also the compactness of metasurface design. Different structures have been proposed so far to answer such demand. Placing an ITO film inside a metal-insulator-metal (MIM) plasmonic cavity, a tunable reflective absorber with up to 15% change in amplitude of reflected light was achieved[25]. A broadband electro-optical modulator based on a multilayer structure was able to attain 37% modulation depth for the reflected light when the incoming light has a 78° incidence angle[26]. A high-efficiency transmittance modulator using ITO-based metasurfaces and hybrid plasmonic waveguide mode has shown a 33% gate-tunable transmittance change by applying a 6 V gate bias[27]. An all-dielectric Huygens metasurface was proposed to control the transmission of light with an on-state transmittance of 70% and a modulation depth of 31%[28]. Moreover, a circular MIM resonator with an ITO film that is polarization insensitive could realize the modulation of transmitted light with a large modulation depth up to 29 dB or 96%[29]. However, all of these metasurfaces comprise a single ITO film with limited modulation depth and their operational wavelength was also restricted to $\lambda \geq$ ~1500 nm in the near-IR spectrum due to the low electron concentration of the deposited ITO film.

Here, a new circular resonator comprising two ITO discs is proposed. We use the coupling of magnetic dipole resonance in the circular resonator with the ENZ wavelength inside the accumulation layer of ITO film to achieve total absorption of reflected light. This is mainly due to the coexistence of magnetic dipole resonance and ENZ wavelength inside the ITO discs. A perovskite high dielectric constant barium strontium titanate (BST) film is sandwiched between two ITO films to increase the electric field and decrease the required voltage. An unprecedented ~84 dB or ~99.99% modulation depth in the reflection mode, insensitive to the polarization of light, was achieved at λ = 820 nm with a single bias voltage of $V = -2.5$ V. The results show a promising way for realizing electrically tunable metasurface for potential high-speed light modulation.

Methods and results

ITO is a conducting material with free electrons which is optically modeled using the Drude model in the visible and near-IR spectra[30]:

$$\tilde{\varepsilon}_{\rm r}(\omega) = \varepsilon_{\rm r}'(\omega) + {\rm i}\varepsilon_{\rm r}''(\omega) = \varepsilon_\infty - \frac{\omega_{\rm p}^2}{\omega^2 + {\rm i}\omega\Gamma}\,, \quad (1)$$

where $\tilde{\varepsilon}_{\rm r}$ is the material permittivity, $\varepsilon_{\rm r}'$ and $\varepsilon_{\rm r}''$ are the real and imaginary parts of the permittivity respectively, ε_∞ is the high-frequency permittivity, ω is the angular frequency, $\omega_{\rm p}$ is the plasma frequency, and Γ is the damping rate. The plasma frequency and damping rate are defined as:

$$\omega_{\rm p}^2 = \frac{N{\rm e}^2}{\varepsilon_0 m^*}\,, \quad (2)$$

$$\Gamma = \frac{1}{\tau} = \frac{\rm e}{\mu m^*}\,, \quad (3)$$

where τ is scattering time, e is the electron charge, μ is the electron mobility, ε_0 is the vacuum permittivity, m^* is the effective electron mass, and N is the electron concentration. By changing the carrier concentration, the plasma frequency changes, thereby changing the dielectric constant. From Eq. (1), the real and imaginary parts of the permittivity are given by:

$$\varepsilon_{\rm r}'(\omega) = \varepsilon_\infty - \frac{\omega_{\rm p}^2}{\omega^2 + \Gamma^2}\,, \quad (4)$$

$$\varepsilon_{\mathrm{r}}^{''}(\omega)=\frac{\Gamma\omega_{\mathrm{p}}^{2}}{\omega\left(\omega^{2}+\Gamma^{2}\right)}\ . \tag{5}$$

The epsilon-near-zero (ENZ) wavelength (λ_{ENZ}) is the wavelength at which the real part of the dielectric constant becomes zero[31,32]. If the imaginary part of the permittivity is zero or near-zero at the same wavelength, the refractive index would become close to zero, much smaller than the refractive index of vacuum. Although common materials, i.e., metals, have $\tilde{\varepsilon}_{\mathrm{r}}=0$ at plasma frequency, the imaginary part of the permittivity is quite large. However, in transparent conductive oxides, the ENZ wavelength can be tuned in the visible and near-IR spectra while having a small value of the imaginary part of the permittivity[33–35]. From Eq. (4), the epsilon-near-zero wavelength (λ_{ENZ}) is given by:

$$\lambda_{\mathrm{ENZ}}=\frac{2\pi c}{\omega_{\mathrm{ENZ}}}=\frac{2\pi c}{\sqrt{\dfrac{\omega_{\mathrm{p}}^{2}}{\varepsilon_{\infty}}-\Gamma^{2}}}\ , \tag{6}$$

where c is the speed of light in the vacuum. It could be seen that changing plasma frequency changes the epsilon-near-zero wavelength. According to Eq. (3), by increasing the electron concentration (N), the plasma frequency (ω_{p}) increases which according to Eq. (6) the epsilon-near-zero wavelength (λ_{ENZ}) decreases.

As a result, to push the tunability of the ITO films to the shorter wavelength and possibly visible spectrum, one needs to increase the electron concentration of the film to above $N=8\times10^{20}$ cm^{-3}. This is validated through the ITO films we deposited using RF magnetron sputtering at room temperature with a deposition rate of 1.1 nm/min. In order to increase the electron concentration, the films were post-annealed at 350 °C using rapid thermal annealing for 3 minutes in a nitrogen atmosphere. Hall measurement and spectroscopic ellipsometry were used to model the electrical and optical properties of the ITO films deposited on quartz and Si substrates, respectively[23]. The electron concentration of the ITO film was increased from $N=3.383\times10^{19}$ cm^{-3} in as-deposited film to $N=8.22\times10^{20}$ cm^{-3} in the post-annealed film. The electrical and optical properties of as-deposited and post-annealed ITO films, from the Drude model, are listed in Table 1. Our films are deposited at room temperature without introducing oxygen to the chamber to increase the oxygen deficiency. Post deposition annealing is performed in a nitrogen atmosphere to further increase the oxygen deficiency and improve crystal quality[36,37].

A dielectric material with a high permittivity would be of great importance to achieve higher capacitance, charge accumulation, and tunability. Unlike the dual-gate structure[22] where an ultrathin 5 nm thick ITO film was sandwiched between two oxide films and two metal electrodes on the sides of the oxide films, we employ a capacitive structure with two 5 nm thick ITO films sandwiching a 50 nm thick perovskite BST film, as shown in Fig. 1. The BST is chosen as the oxide film due to its high dielectric constant ($\varepsilon_{\mathrm{DC}}>500$ at room temperature) which would increase the total capacitance and charge accumulation in the ITO films[38]. Considering an electric field of $E=500$ kV/cm, the applied voltage would be equal to $V=2.5$ V. We keep the thickness of the ITO films as low as possible (5 nm) which would increase the amount of achievable modulation[22].

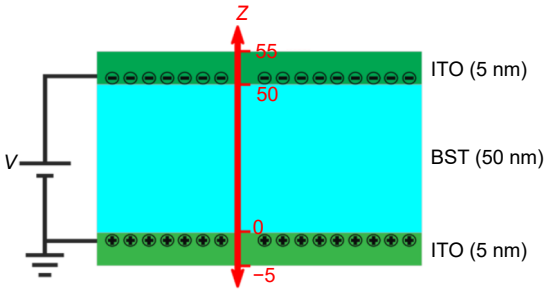

Fig. 1 | Schematic of the tunable double ITO capacitive structure.

The parameters for the ITO films are taken from the post-annealed 5 nm film shown in Table 1 as $N=8.22\times10^{20}$ cm^{-3}, $\mu=21$ cm^2/(V·s), $m^*=0.26m_{\mathrm{e}}$, and $\varepsilon_{\infty}=4.0212$. This film has a plasma frequency of $\omega_{\mathrm{p}}=3.177\times10^{15}$ rad/s and damping constant of $\Gamma=3.232\times10^{14}$ rad/s, as calculated using Eqs. (2) and (3), respectively. These data are used to do electrical charge simulations using Lumerical Device software. The capacitive structure is simulated in a 2D setup and the applied DC voltage between the two ITO films is decreased from $V=0$ V to $V=-2.5$ V. In simulations, the unstructured tetrahedral finite-element mesh with a minimum edge length of 0.1 nm is used for ITO films.

The simulated electron concentration for the top and bottom ITO film along the ITO film thickness versus the bias voltage is shown in Fig. 2. The electron concentration is calculated using a charge monitor placed along the Z axis as shown in red color in Fig. 1. The bottom of BST film is considered as $Z=0$, the top ITO film would be at 50 nm $< Z <$ 55 nm, and the bottom ITO film would be at -5 nm $< Z <$ 0 nm. Under $V=0$ V bias

Table 1 | Electrical and optical properties of the ITO films.

Sample	Sheet resistivityρ (Ω/sq)	Electron mobility μ (cm²/(V·s))	Electron concentration N (cm^{-3})	High-frequency permittivity ε_∞	Effective electron mass $m^*(m_e)$	Plasma Frequency ω_p (rad/s)	Damping rate Γ (rad/s)	ENZ wavelength λ_{ENZ} (μm)
As-deposited	2.94 × 10^4	12.6	3.383 × 10^{19}	4.3968	0.22	6.996 × 10^{14}	6.345 × 10^{14}	>10
Post-annealed	724.6	21	8.220 × 10^{20}	4.0212	0.26	3.177 × 10^{15}	3.232 × 10^{14}	1.214

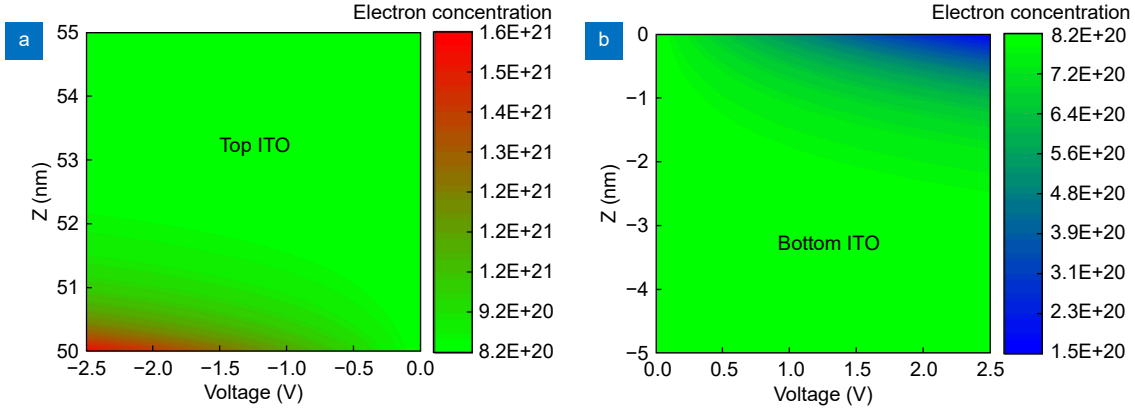

Fig. 2 | Electron concentrations in the (**a**) top and (**b**) bottom ITO films as functions of the applied voltage. The electron concentration along the Z axis, 50 nm < Z < 55 nm in the top ITO film and −5 nm < Z < 0 nm in the bottom ITO film. The initial electron concentration for both films equal to N_0 = 8.22 × 10^{20} cm^{-3} is shown in green color. The increased electron concentration is shown with red color in the accumulation layer of the top ITO film and the decreased electron concentration is shown with blue color in the depletion layer of the bottom ITO film.

voltage, the electron concentration is $N_0 = 8.22\times 10^{20}$ cm^{-3} along the both ITO films thickness as shown in green color in Fig. 2(a) and 2(b). By increasing the negative voltage on the top ITO film in Fig. 1, the electrons accumulate on the interface of ITO with dielectric BST film, creating an accumulation layer of electrons inside the top ITO film. As shown with red color in Fig. 2(a), the electron concentration is increased from $N_0 = 8.22 \times 10^{20}$ cm^{-3} to a maximum of $N_a = 1.62\times 10^{21}$ cm^{-3} inside the accumulation layer. On the other hand, as shown with blue color in Fig. 2(b), the electron concentration is decreased inside the bottom ITO film at the ITO/BST interface as the voltage is increased, creating a depletion layer of electrons. The electron concentration inside this depletion layer is decreased from $N_0 = 8.22 \times 10^{20}$ cm^{-3} to a minimum of $N_d = 1.55\times 10^{20}$ cm^{-3}. According to the simulation results shown in Fig. 2, the effective thickness of accumulation and depletion layers, which would affect the optical performance of the device, are approximately 0.5 nm and 1 nm under the bias voltages of $V = -2.5$ V and $V = 2.5$ V, respectively. As a result, the thicknesses of the accumulation and depletion layers, the tunable part of ITO films, are considered as 1 nm for the following optical simulation of the metasurface. After post-annealing, the ITO films are in the crystalline/polycrystalline phase, a particularly complex crystal structure with about 80 atoms per unit cell, with a lattice constant of ~1.01 nm[39,40]. In ITO film with such a high electron concentration, a degenerated gas of current-carrying electrons is created via chemical doping of tin for indium and increased by the presence of oxygen vacancy impurity states[30]. As a result, the 1 nm tunable layer of ITO film is divided into two 0.5 nm layers in which each layer has a different electron concentration estimated from simulation results shown in Fig. 2.

Plasma frequency (ω_p) and damping rate (Γ) for ITO film, accumulation and depletion layers are calculated using the N_0, N_a, and N_d from Eqs. (2) and (3). These values are used to calculate real and imaginary parts of the permittivity from Eqs. (4) and (5). Then, the refractive index (n) and extinction coefficient (κ) are calculated from complex refractive index as $\tilde{n}^2 = (n + i\kappa)^2 = \tilde{\varepsilon}_r\tilde{\mu}_r$, where $\tilde{\mu}_r$ is the complex relative permeability. Since ITO is a non-magnetic material at optical frequencies, its relative permeability is equal to 1. The refractive index and extinction coefficients values could be deduced as:

$$n(\omega) = \sqrt{\frac{\sqrt{\varepsilon_r'^2 + \varepsilon_r''^2} + \varepsilon_r'}{2}}, \qquad (7)$$

$$\kappa(\omega)=\sqrt{\frac{\sqrt{\varepsilon_{\rm r}'^{2}+\varepsilon_{\rm r}''^{2}}-\varepsilon_{\rm r}'}{2}}\,. \tag{8}$$

Since for the ITO film the $\varepsilon_{\rm r}''$ has small values near the $\lambda_{\rm ENZ}$, where the $\varepsilon_r'=0$, the minimum value of $n(\omega)$ would be near $\lambda_{\rm ENZ}$. The optical properties of the ITO in three states, un-biased ($N_0=8.22\times10^{20}$), accumulation ($N_{\rm a}=1.62\times10^{21}$), and depletion ($N_{\rm d}=1.55\times10^{20}$) layers are shown in Fig. 3 with green, red, and blue color lines, respectively. Other parameters are taken from Table 1 as $\mu=21$ cm^2/(V·s), $m^*=0.26m_{\rm e}$, and $\varepsilon_\infty=4.0212$, similar for all three states.

As shown in Fig. 3(a), the epsilon-near-zero wavelength ($\lambda_{\rm ENZ}$) of the ITO film (N_0), where the green line crosses zero, is around $\lambda=1.2$ μm. After applying bias voltage, the ENZ wavelength blue-shifts to $\lambda=820$ nm inside the accumulation layer and red-shifts to $\lambda>2$ μm inside the depletion layer. As the $\lambda_{\rm ENZ}$ moves toward shorter wavelength, the loss (imaginary part of the permittivity) is increased in the visible spectrum, as shown in Fig. 3(b). By increasing the electron concentration inside the accumulation layer, the plasma frequency is increased (Eq. (2)) and the imaginary part of the permittivity is also increased (Eq. (5)). On the other hand, the imaginary part of the permittivity and loss is decreased as the electron concentration is decreased.

Figure 3(c) and 3(d) show the refractive index and extinction coefficient of ITO in three different states. As explained before, the dip in the refractive index spectrum, which would be near the ENZ wavelength, blue-shifts toward the visible spectrum in the accumulation layer of the film, and red-shifts in the depletion layer to wavelength longer than $\lambda=2$ μm. It could be seen from the extinction coefficient that the ITO film becomes lossier in the accumulation layer and more transparent in the depletion layer. In other words, the accumulation layer is more metallic and lossy with more electron concentration and the depletion layer is more dielectric and transparent as it is less conductive.

One approach for designing the tunable metasurfaces could be taking advantage of significant change in the refractive index as shown in Fig. 3(c). However, this

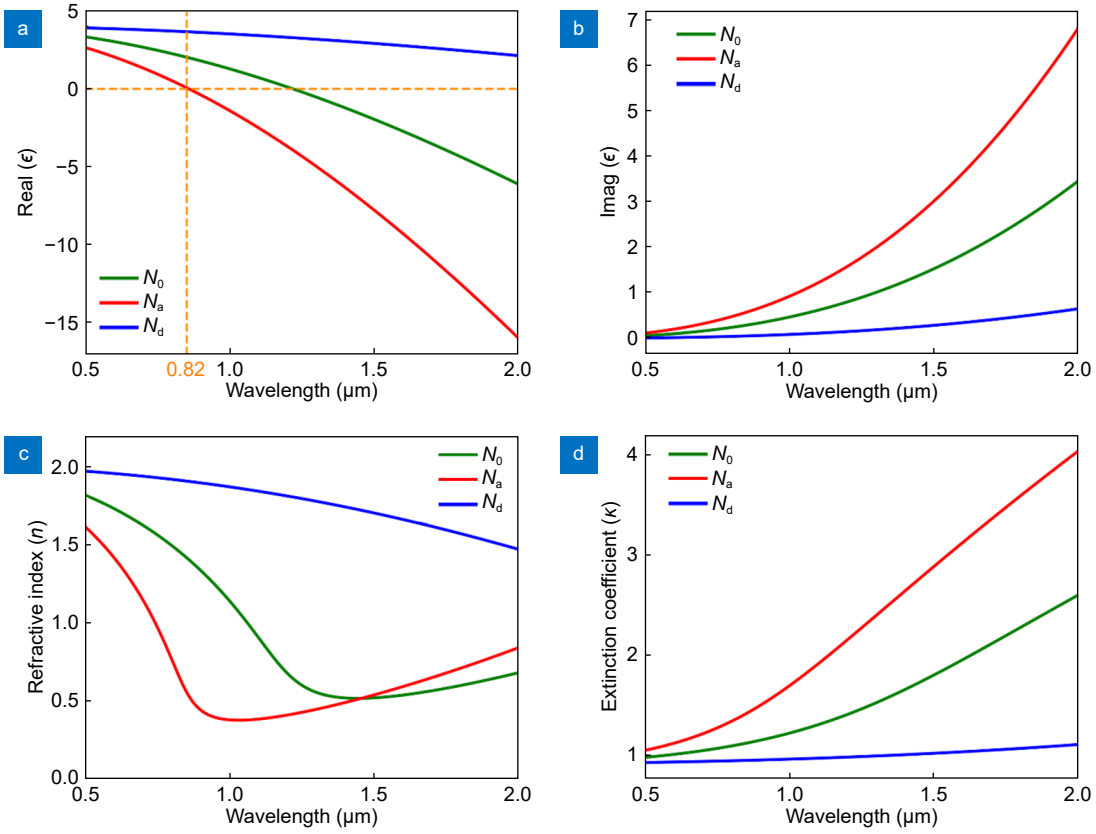

Fig. 3 | Optical properties of ITO film as functions of the applied voltage. The optical properties of the ITO film interface with the BST film in three different conditions. $N_{\rm a}$ represents the optical property of the accumulation layer, $N_{\rm d}$ represents the optical property of the depletion layer, and N_0 represents the optical property of interface without bias voltage (un-biased) and all other parts of the ITO film. (**a**) The real part of the permittivity $\varepsilon_{\rm r}'(\omega)$. (**b**) The imaginary part of the permittivity $\varepsilon_{\rm r}''(\omega)$. (**c**) Refractive inde n, and (**d**) the extinction coefficient of the ITO film κ.

change only happens in very thin (~1 nm) accumulation and depletion layers. The better approach would be making use of the tunability of ENZ wavelength in the accumulation and depletion layers. The electric field would accumulate and intensify inside the ENZ layer and result in significant phase and intensity modulation[34,35]. However, these tunable metasurfaces suffer from low efficiency due to the inherent high loss of accumulation layer[22,41], as shown in Fig. 3(b) and 3(d). In other words, the total efficiency of the metasurface is limited by the ohmic loss of the ITO film. Here, this ohmic loss is going to be used as an advantage to design a reflective modulator using double ITO films. The modulator would have two states of ON and OFF. In the ON state, the reflection amplitude would be the maximum with ENZ wavelength far away from the operational wavelength. In the OFF state, the reflection amplitude would decrease dramatically due to the high loss with ENZ shifting to the operational wavelength.

Figure 4 shows the unit cell of such electrically controlled modulator metasurface comprising a 100 nm thick silver mirror, circular-shaped ITO-BST-ITO resonator, and silicon resonator with $D = 250$ nm diameter, and four $W = 20$ nm wide bias connections on the sides of resonators. The ITO, BST, and Si films are $t_{ITO} = 5$ nm, $t_{BST} = 50$ nm, and $t_{Si} = 50$ nm thick, respectively. All the top ITO discs are connected through the top ITO film in bias connections. All the bottom ITO discs are electrically connected through the bottom Ag mirror and bottom ITO film in bias connections. A single voltage source is used to control the charge accumulation and depletion in the ITO discs, as shown in Fig. 4(b), and tune the reflection amplitude of the light. Such a metasurface could be fabricated by using ebeam lithography (EBL) and conventional semiconductor processing. For example, a 100 nm thick Ag film could be deposited using ebeam evaporation on a highly doped Si substrate to allow the bottom ITO film to be addressed electrically through the substrate. Then the bottom ITO, BST, top ITO, and Si films would be deposited using RF sputtering. The nano-disc structure could be created by EBL patterning and plasma or deep reactive ion etching (DRIE) by using an appropriate masking layer. A post-annealing would be performed to increase the electron concentration of ITO films.

Due to the circular shape of the resonator and symmetrical design of the bias connections on the four sides of the resonator, the modulator metasurface is insensitive to the polarization of incident light, explained in detail in another work[29]. The performance of the modulator metasurface is simulated using Lumerical FDTD software. A single unit cell with periodic boundary conditions is simulated to numerically calculate the reflection amplitude of the modulator metasurface. A local mesh cell with dimensions of $dx \times dy \times dz = 5\ \text{nm} \times 5\ \text{nm} \times 0.5\ \text{nm}$ is chosen for ITO discs to accurately model the accumulation and depletion layers. The ITO film is modeled using the Drude model with the properties measured and explored previously. The first 1 nm thick layer of the ITO films at the interface with BST film is considered as the tunable accumulation/depletion layers. The electron concentration of the first 0.5 nm near BST film is changed from N_0 to N_a or N_d according to the applied voltage, while the next 0.5 nm is changed

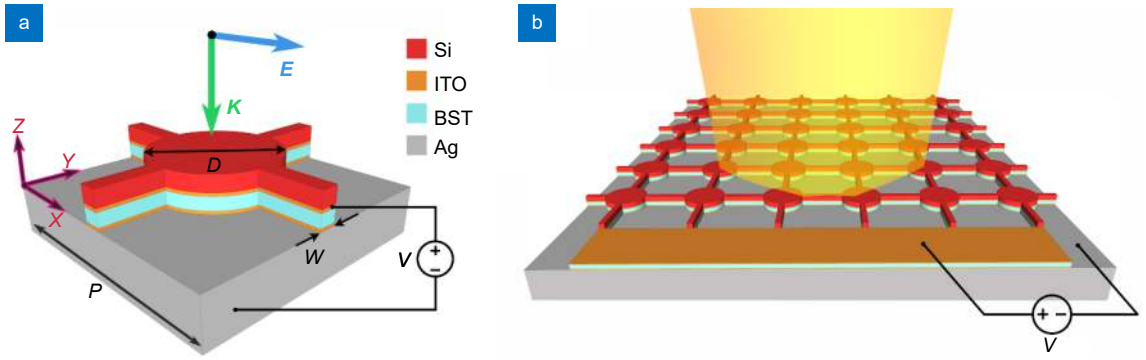

Fig. 4 | Schematic of the electrically controlled reflective modulator metasurface. (**a**) A square unit cell is constructed from a circular silicon resonator on the top of a circular ITO-BST-ITO resonator on the top of a silver mirror. Four symmetrical bias connections with the same layers are used to make bias connections between the ITO films. Parameter values are t_{Ag} =100 nm, t_{ITO} = 5 nm, t_{BST} = 50 nm, t_{Si} = 50 nm, W = 20 nm, D = 250 nm, and P = 520 nm. The initial polarization of light is shown along the X axis. (**b**) 3D schematic of the metasurface constructed from a 6×6 array of unit cells. The metasurface is controlled by applying the voltage between the bottom silver film (grey) and the top ITO electrode (orange). The electrical current passes to the resonators through a 2D array of bias connections.

according to the applied voltage and simulation results in Fig. 2 to accurately model the accumulation (0.5 nm) and depletion (1 nm) layers. Under $V = 0$ V bias voltage (ON state), the electron concentration of both layers is considered N_0. Under $V = 2.5$ V bias voltage (OFF state 1), the electron concentration of the top 0.5 nm tunable layer is changed to N_d (depletion layer) and the bottom 0.5 nm tunable layer to N_a (accumulation layer), while under $V = -2.5$ V bias voltage (OFF state 2), the electron concentration in the top 0.5 nm tunable layer is changed to N_a and the bottom 0.5 nm tunable layer to N_d.

Simulated reflection spectra of the modulator under three different voltages $V = -2.5, 0$ and 2.5 V are shown in red, green, and blue colors, respectively, in Fig. 5(a). As explained before, the operational wavelength is set at the ENZ wavelength of the accumulation layer, $\lambda = 820$ nm, to get the strongest resonance and thus the highest loss and the largest modulation depth. The reflection amplitude at $\lambda = 820$ nm under $V = 0$ V is 56.3%. It is a dip in the reflection spectra mainly due to magnetic dipole resonance in the ITO-BST-ITO resonator. By decreasing the voltage to $V = -2.5$ V (OFF state 2), the accumulation layer is created at the bottom of the top ITO film which drops the reflection down to 3.58×10^{-3}%. This is due to the coexistence of magnetic dipole resonance and ENZ wavelength inside the accumulation layer at this wavelength. If the voltage is reversed to $V = 2.5$ V, the accumulation layer is created in the bottom ITO film and the reflection amplitude drops to 4.2% (OFF state 1). As the distance between the accumulation layer and the silver ground plane is changed, the resonance wavelength is slightly changed and the resonance strength is slightly weakened. The modulation depth (MD) is defined as:

$$MD = 20\log\left(R_{Max}/R_{Min}\right), \tag{9}$$

where $R_{Min} = 3.58 \times 10^{-3}$% and $R_{Max} = 56.3$% are the minimum and maximum reflection amplitudes before (ON state) and after (OFF state 2) applying the bias voltage, respectively, at $\lambda = 820$ nm. Hence, under $V = -2.5$ V the proposed modulator metasurface achieves 84 dB modulation depth, equal to ~99.99%, if defined as $MD = (|\Delta R|/R_{Max}) \times 100$. Under $V = -2.5$ V, where the accumulation layer is created in the top ITO film, the reflection amplitude remains below 1% (MD ~40 dB) in the range of 805 nm $< \lambda <$ 835 nm and remains below 5% (MD ~22 dB) in the range of 795 nm $< \lambda <$ 850 nm. Under $V = 2.5$ V, where the accumulation layer is created in the bottom ITO film, the reflection amplitude remains below 1% in the range of 790 nm $< \lambda <$ 860 nm and below 5% in the range of 785 nm $< \lambda <$ 870 nm.

To investigate the phenomena behind such ultra-high modulation depth, the electric field inside the resonator is studied at the resonance wavelength (λ = 820 nm). The electric field intensity under three different bias voltages is shown in Fig. 6. A field monitor is placed along the *XZ* plane, according to Fig. 4, in the middle of the circular resonator. Under $V = 0$ V bias voltage, it could be seen in Fig. 5 that there was a small dip in the reflection spectrum at λ = 820 nm indicating a slight resonance in the

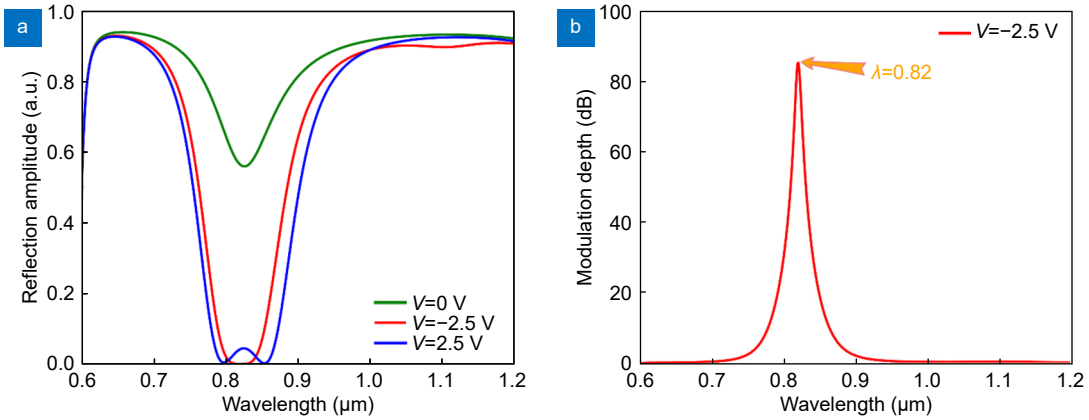

Fig. 5 | Performance of the electrically tunable modulator metasurface. (**a**) Simulated reflection spectra of the modulator under three different voltages. Under V = 0 V bias voltage, both ITO films have an electron concentration of N_0. Under V = −2.5 V, the top ITO film has a 0.5 nm thick accumulation layer with an electron concentration of N_a and the bottom ITO film has a 1 nm thick depletion layer with an electron concentration of N_d. Under V = 2.5 V, the top ITO film has a depletion layer with an electron concentration of N_d and the bottom ITO film has an accumulation layer with an electron concentration of N_a. (**b**) Modulation depth spectra of modulator under V = −2.5 V. The modulation depth peaks to ~84 dB at the wavelength of λ = 820 nm.

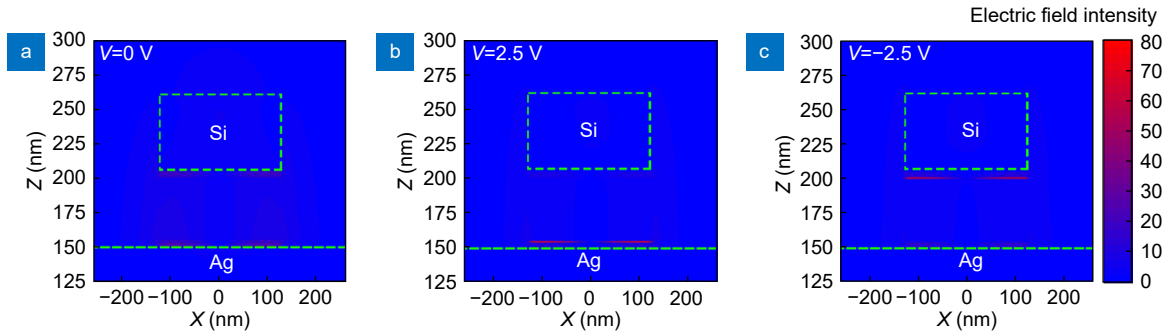

Fig. 6 | Electric field intensity along *XZ* plane under the bias voltages of (**a**) V = 0 V at λ = 820 nm, (**b**) V = 2.5 V at λ = 800 nm, and (**c**) V = −2.5 V at λ = 820 nm. The edges of the Si disc and silver mirror are shown with green dashed lines.

resonator. The cause of that resonance could be seen in Fig. 6(a), as the electric field is confined inside the top and bottom ITO discs. As explained earlier, ITO films are modeled using the Drude model with electron concentration $N_0 = 8.22 \times 10^{20}$ cm^{-3}, implying semi-metallic properties of the ITO in visible and near-IR spectra. Moreover, the ENZ wavelength of un-biased ITO film was calculated in Table 1 as λ_{ENZ} ~1.2 μm, relatively close to the wavelength of geometrical resonance, implying a weak ENZ resonance inside the top and bottom circular ITO discs. This geometrical resonance is a magnetic dipole resonance which would be explored in Fig. 7. By changing the voltage to $V = 2.5$ V, the accumulation layer is created in the bottom ITO layer interfacing the BST, as shown in Fig. 6(b). This accumulation layer has the ENZ wavelength at λ = 820 nm which was the resonance wavelength of the magnetic dipole resonator. A combination of the electric field enhancement in the ENZ layer and magnetic dipole resonance confines the light inside the 0.5 nm thick ITO accumulation layer. This could also be explained as a narrow channel with a deep subwavelength transverse cross-section made of ENZ material, in the resonance wavelength[42]. As shown in Fig. 3(b) and 3(d), at the ENZ wavelength the accumulation layer becomes very lossy. This strong resonance and confinement of the light inside a very thin accumulation layer cause total loss of the light with almost no reflection, acting similar to a complete absorber. As shown in Fig. 5(a), due to the short distance between the ENZ resonator and the ground plane, there are two identical magnetic dipole resonances around λ = 820 nm resulting in two dips at λ = 795 nm and λ = 845 nm[25].

As shown in Fig. 6(c), the same phenomenon happens at $V = -2.5$ V but the accumulation layer is created inside the top ITO film interfacing with the BST disc. It is important to note that as the accumulation layer is created inside one ITO disc, the depletion layer is created in the other ITO disc. The depletion layer has a much lower electron concentration and its ENZ wavelength redshifts to $\lambda > 2$ μm. This results in lower electric field confinement compared to the un-biased ITO film and accumulation layer, which could be seen in Fig. 6.

To further investigate the resonance inside the accumulation layer, a field monitor is placed along the *XY* plane inside the accumulation layer in the top ITO film under a bias voltage of $V = -2.5$ V. The electric and magnetic fields at λ = 820 nm are shown in Fig. 7.

The electric and magnetic field intensities in the *XY* plane inside the accumulation layer are shown in Fig. 7(a) and 7(b). The magnetic field looks like an ellipse stretched along the *Y* axis, while the electric field is stronger on the left and right side of the ENZ region where the magnetic field is the weakest. This is in agreement with the polarization of light, where the electric field was along the *X* axis and the magnetic field along the *Y* axis, as shown in Fig. 4(a). The top and side views of the electric field vectors are shown in Fig. 7(c) and 7(e), respectively. The electric field vectors represent an electric current in the shape of a stretched circular loop, antiparallel on two sides of the ENZ region. The top and side views of the magnetic field vectors are shown in Fig. 7(d) and 7(f). The magnetic field vectors are stretched along the positive *Y* direction in the center of the ENZ region, strongest in the center of the ENZ region where the electric field is the weakest. All of this implies a magnetic dipole stretched along the *Y* axis is created inside the accumulation layer.

Figure 8 shows the impact of the Si disc thickness on the reflection spectra under the bias voltages of V = 0 V and $V = -2.5$ V. As shown in Fig. 8(a), under the bias voltage of V = 0 V, the wavelength of the magnetic dipole resonance is increasing from 630 nm to 820 nm as

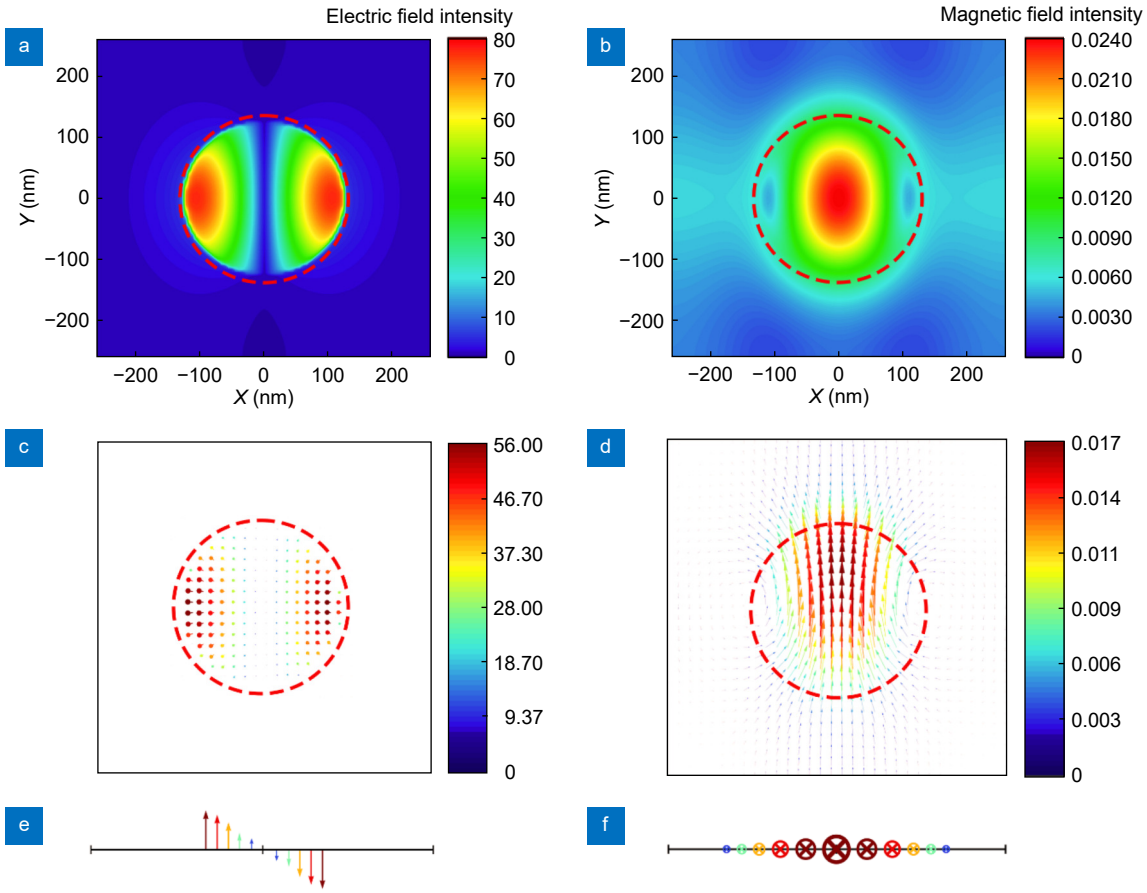

Fig. 7 | The electric and magnetic fields under a bias voltage of $V = -2.5$ V inside the accumulation layer at $\lambda = 820$ nm. (**a**) Electric and (**b**) magnetic field intensities in the *XY* plane inside the accumulation layer in the top ITO film. Top view of the vectors of the (**c**) electric and (**d**) magnetic fields from the same monitor. Side view of the vectors of the (**e**) electric and (**f**) magnetic fields from the same monitor. The vector figures (e) and (f) share the same scalar bar as vector figures (c) and (d), respectively. The edge of the ITO disc is shown by the red dashed lines.

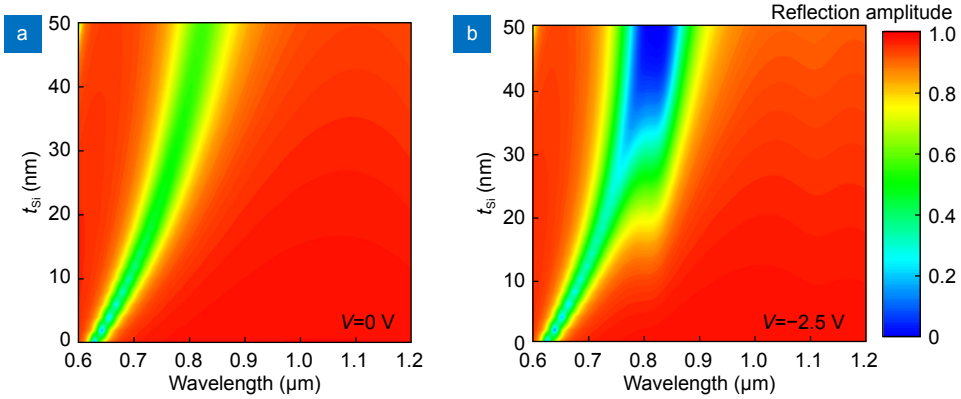

Fig. 8 | Impact of the Si disc thickness on the reflection spectra. Map of the reflection spectra of the modulator metasurface with a varying thickness of the Si disc (0 nm ≤ t_{Si} ≤ 50 nm) under the bias voltages of (**a**) $V = 0$ V and (**b**) $V = -2.5$ V.

the thickness of Si disc is increased from 0 to 50 nm. Moreover, the FWHM of the resonance is increasing from ~15 nm at $t_{Si} = 0$ nm to ~100 nm at $t_{Si} = 50$ nm. As shown in Fig. 8(b), under the bias voltage of $V = -2.5$ V, the reflection spectra are similar to Fig. 8(a) without bias voltage. However, as the thickness of the Si disc is increased above 20 nm, a new resonance with a slightly longer wavelength appears in the reflection spectra. The minimum reflection at the dip of spectra becomes nearly zero for $t_{Si} \geq 40$ nm. This could be explained by the coexistence of ENZ wavelength by two neighboring magnetic dipole resonances. Moreover, the effect of polarization of

incident light, angle of the incident light with the surface normal, the width of the bias connections, and ITO discs thickness are explored and the simulation results could be found in the Supplemental Material.

The operational wavelength of the modulator is the result of the coexistence of magnetic dipole resonance and ENZ wavelength. Hence, both of them should be shifted to change the operational wavelength of the modulator. The wavelength of magnetic dipole resonance could be tuned by changing the diameter of the resonator. For example, by increasing the diameter of the circular resonator, the wavelength of magnetic dipole resonance would increase. In such a case, the ENZ wavelength of the accumulation layer inside the ITO film also should be increased to this new longer wavelength. This could be achieved by either applying a smaller voltage between the ITO films or choosing an ITO film with a lower initial electron concentration (longer initial ENZ wavelength). However, decreasing the operational wavelength is not possible. The magnetic dipole resonance wavelength could be reduced by decreasing the diameter of the resonator. However, decreasing the ENZ wavelength of the accumulation layer is not possible since it requires an increase in the initial electron concertation of the deposited ITO films which according to our experiments is maxed out at 8.22×10^{20} cm^{-3} for 5 nm ITO film. Note that increasing the applied voltage to further blue-shift the ENZ wavelength is not an answer since it may cause the breakdown of BST film due to extremely high dielectric field.

Conclusion

An electrically tunable polarization-insensitive modulator metasurface operating in reflection mode was proposed. It has a tunable capacitive structure comprising a high dielectric constant perovskite BST film sandwiched between two ultra-thin 5 nm ITO films. These ITO films act as active tuning media through electron accumulation/depletion and also the electrodes for applying the bias voltage. The coupling of magnetic dipole resonance with the ENZ wavelength inside the accumulation layer was used to achieve the total absorption of reflected light. The metasurface achieved 84 dB or ~99.99% modulation depth at the operation wavelength of $\lambda = 820$ nm and ~40 dB in the wavelength range of 805 nm $< \lambda <$ 835 nm under $V = -2.5$ V. By designing circular resonators and symmetrical 2D bias connections, the metasurface was insensitive to the polarization of the incident light. The proposed tunable metasurface could potentially be used for the active control of the light intensity with fast electrical signal modulation in the visible and near-IR spectra as a tunable flat optical interconnect, switch, and sensing device.

References

1. Holloway CL, Kuester EF, Gordon JA, O'Hara J, Booth J et al. An overview of the theory and applications of metasurfaces: the two-dimensional equivalents of metamaterials. *IEEE Antenn Propag Mag* **54**, 10–35 (2012).
2. Yu NF, Capasso F. Flat optics with designer metasurfaces. *Nat Mater* **13**, 139–150 (2014).
3. Kildishev AV, Boltasseva A, Shalaev VM. Planar photonics with metasurfaces. *Science* **339**, 1232009 (2013).
4. Zhang YB, Liu H, Cheng H, Tian JG, and Chen SQ. Multidimensional manipulation of wave fields based on artificial microstructures. *Opto-Electron Adv* **3**, 200002 (2020).
5. Ni XJ, Kildishev AV, Shalaev VM. Metasurface holograms for visible light. *Nat Commun* **4**, 2807 (2013).
6. Khorasaninejad M, Chen WT, Devlin RC, Oh J, Zhu AY et al. Metalenses at visible wavelengths: Diffraction-limited focusing and subwavelength resolution imaging. *Science* **352**, 1190–1194 (2016).
7. Ma XL, Pu MB, Li X, Guo YH, Luo XG. All-metallic wide-angle metasurfaces for multifunctional polarization manipulation. *Opto-Electron Adv 2* , 180023 (2019).
8. Glybovski SB, Tretyakov SA, Belov PA, Kivshar YS, Simovski CR. Metasurfaces: from microwaves to visible. *Phys Rep* **634**, 1–72 (2016).
9. Nemati A, Wang Q, Hong MH, Teng JH. Tunable and reconfigurable metasurfaces and metadevices. *Opto-Electron Adv* **1**, 180009 (2018).
10. Brar VW, Jang MS, Sherrott M, Lopez JJ, Atwater HA. Highly confined tunable mid-infrared plasmonics in graphene nanoresonators. *Nano Lett* **13**, 2541–2547 (2013).
11. Sherrott MC, Hon PWC, Fountaine KT, Garcia JC, Ponti SM et al. Experimental demonstration of > 230° phase modulation in gate-tunable graphene–gold reconfigurable mid-infrared metasurfaces. *Nano Lett* **17**, 3027–3034 (2017).
12. Ooi KJA, Leong PC, Ang LK, Tan DTH. All-optical control on a graphene-on-silicon waveguide modulator. *Sci Rep* **7**, 12748 (2017).
13. Guo JY, Wang T, Quan BG, Zhao H, Gu CZ et al. Polarization multiplexing for double images display. *Opto-Electron Adv 2* , 180029 (2019).
14. Dou KH, Xie X, Pu MB, Li X, Ma XL et al. Off-axis multi-wavelength dispersion controlling metalens for multi-color imaging. *Opto-Electron Adv 3* , 190005 (2020).
15. Gao JW, Kempa K, Giersig M, Akinoglu EM, Han B et al. Physics of transparent conductors. *Adv Phys* **65**, 553–617 (2016).
16. Chopra KL, Major S, Pandya DK. Transparent conductors—a status review. *Thin Solid Films* **102**, 1–46 (1983).
17. Babicheva VE, Boltasseva A, Lavrinenko AV. Transparent conducting oxides for electro-optical plasmonic modulators. *Nanophotonics* **4**, 165–185 (2015).
18. Ou JY, Plum E, Zhang JF, Zheludev NI. An electromechanically reconfigurable plasmonic metamaterial operating in the

near-infrared. *Nat Nanotechnol* **8**, 252–255 (2013).
19. Ee HS, Agarwal R. Tunable metasurface and flat optical zoom lens on a stretchable substrate. *Nano Lett* **16**, 2818–2823 (2016).
20. Liu L, Kang L, Mayer TS, Werner DH. Hybrid metamaterials for electrically triggered multifunctional control. *Nat Commun* **7**, 13236 (2016).
21. ForouzmA, Salary MM, Inampudi S, Mosallaei H. A tunable multigate Indium‐Tin‐oxide‐assisted all‐dielectric metasurface. *Adv Opt Mater* **6**, 1701275 (2018).
22. Kafaie Shirmanesh G, Sokhoyan R, Pala RA, Atwater HA. Dual-gated active metasurface at 1550 nm with wide (> 300°) phase tunability. *Nano Lett* **18**, 2957–2963 (2018).
23. Huang YW, Lee HW, Sokhoyan R, Pala RA, Thyagarajan K et al. Gate-tunable conducting oxide metasurfaces. *Nano Lett* **16**, 5319–5325 (2016).
24. Park J, Jeong BG, Kim SI, Lee D, Kim J et al. All-solid-state spatial light modulator with independent phase and amplitude control for three-dimensional LiDAR applications. *Nat Nanotechnol* **16**, 69–76 (2021).
25. Park J, Kang JH, Liu XG, Brongersma ML. Electrically tunable epsilon-near-zero (ENZ) metafilm absorbers. *Sci Rep* **5**, 15754 (2015).
26. Shi KF, Haque RR, Zhao BY, Zhao RC, Lu ZL. Broadband electro-optical modulator based on transparent conducting oxide. *Opt Lett* **39**, 4978–4981 (2014).
27. Lee Y, Yun J, Kim SJ, Seo M, In S et al. High‐speed transmission control in gate‐tunable metasurfaces using hybrid plasmonic waveguide mode. *Adv Opt Mater* **8**, 2001256 (2020).
28. Howes A, Wang WY, Kravchenko I, Valentine J. Dynamic transmission control based on all-dielectric Huygens metasurfaces. *Optica* **5**, 787–792 (2018).
29. Nemati A, Qian W, Hong MH, Teng JH. Electrically tunable polarization-insensitive MIM plasmonic metasurface operating in transmission mode. *J Opt* **21**, 055102 (2019).
30. Edwards PP, Porch A, Jones MO, Morgan DV, Perks RM. Basic materials physics of transparent conducting oxides. *Dalton Trans* **19**, 2995–3002 (2004).
31. Alù A, Silveirinha MG, Salandrino A, Engheta N. Epsilon-near-zero metamaterials and electromagnetic sources: Tailoring the radiation phase pattern. *Phys Rev B* **75**, 155410 (2007).
32. Liberal I, Engheta N. The rise of near-zero-index technologies. *Science* **358**, 1540–1541 (2017).
33. Naik GV, Kim J, Boltasseva A. Oxides and nitrides as alternative plasmonic materials in the optical range[Invited]. *Opt Mater Express* **1**, 1090–1099 (2011).
34. Kinsey N, DeVault C, Boltasseva A, Shalaev VM. Near-zero-index materials for photonics. *Nat Rev Mater* **4**, 742–760 (2019).
35. Lobet M, Liberal I, Knall EN, Alam MZ, Reshef O et al. Fundamental radiative processes in near-zero-index media of various dimensionalities. *ACS Photonics* **7**, 1965–1970 (2020).
36. Chen AQ, Zhu KG, Zhong HC, Shao QY, Ge GL. A new investigation of oxygen flow influence on ITO thin films by magnetron sputtering. *Solar Energy Mater Solar Cells* **120**, 157–162 (2014).
37. Izumi H, Adurodija FO, Kaneyoshi T, Ishihara T, Yoshioka H et al. Electrical and structural properties of indium tin oxide films prepared by pulsed laser deposition. *J Appl Phys* **91**, 1213–1218 (2002).
38. Gorzkowski EP, Pan MJ, Bender B, Wu CCM. Glass-ceramics of barium strontium titanate for high energy density capacitors. *J Electroceram* **18**, 269–276 (2007).
39. Vidhya VS, Malathy V, Balasubramanian T, Saaminathan V, Sanjeeviraja C et al. Influence of RF power on the growth mechanism, preferential orientation and optoelectronic properties of nanocrystalline ITO films. *Curr Appl Phys* **11**, 286–294 (2011).
40. Fan JCC, Goodenough JB. X‐ray photoemission spectroscopy studies of Sn‐doped indium‐oxide films. *J Appl Phys* **48**, 3524–3531 (1977).
41. Forouzmand A, Salary MM, Shirmanesh GK, Sokhoyan R, Atwater HA et al. Tunable all-dielectric metasurface for phase modulation of the reflected and transmitted light via permittivity tuning of indium tin oxide. *Nanophotonics* **8**, 415–427 (2019).
42. Silveirinha MG, Engheta N. Theory of supercoupling, squeezing wave energy, and field confinement in narrow channels and tight bends using ε near-zero metamaterials. *Phys Rev B* **76**, 245109 (2007).

Acknowledgements

This work is supported by the Agency for Science, Technology and Research (A*STAR) under AME IRG Grant No. A2083c0058, AME IAF-PP Grant No. 182 24 30030, HBMS IAF-PP Grant No. H19H6a0025, and by MOE Tier 3 program LUNI170919aPUBMOE.

Competing interests

The authors declare no competing financial interests.

Supplementary information

Supplementary information for this paper is available at https://doi.org/10.29026/oea.2021.200088